Clin Neuroradiol (2022) 32:507–515
https://doi.org/10.1007/s00062-021-01076-4

ORIGINAL ARTICLE

Diagnostic Performance of MRA for UnrupturedAneurysms at the Distal ICA

Guangchen He[1] · Jienan Wang[1] · Yiran Zhang[1] · Minghua Li[1] · Haitao Lu[1] · Yingsheng Cheng[1] · Yueqi Zhu[1]

Received: 13 April 2021 / Accepted: 21 July 2021 / Published online: 24 January 2022

Abstract

Purpose Unruptured intracranial aneurysms (UIAs) at the distal internal carotid artery (ICA) (segments C5–C7) are difficult to accurately display on computed tomography angiography (CTA) due to the influences of bone structures and vessel curvature. We investigated the utility of three-dimensional time-of-flight magnetic resonance angiography (3D-TOF-MRA) at 3.0-T for the detection of morphologic features compared to digital subtraction angiography (DSA).

Methods This retrospective study included 2398 patients between January 2015 and May 2020 who underwent 3D-TOF-MRA and DSA within 3 months. Morphologic features including aneurysm size, neck width, shape and relation to adjacent arteries and other diagnostic parameters were recorded. Three observers blinded to the clinical and DSA results independently analyzed MRA data sets. The statistical difference of each aneurysm-specific variable was performed using χ^2-tests and multivariate logistic regression analysis.

Results A total of 551 aneurysms in 514 patients were confirmed at the distal ICA by DSA. Patient-based, aneurysm-based and location-based evaluations with 3D-TOF-MRA yielded high diagnostic accuracy in the detection of target UIAs. The accuracy of displayed morphologic features was 94.9% for size, 97.2% for neck width, 92.6% for shape, and 96.4% for relationship to adjacent vessels. Multivariate logistic regression showed that tiny ($P<0.001$) or giant ($P=0.039$) size and a lobulated shape ($P=0.006$) significantly affected the morphologic assessment on 3D-TOF-MRA.

Conclusion Three-dimensional TOF-MRA can accurately depict and display morphologic features of distal ICA UIAs. Tiny or giant-sized distal ICA aneurysms and with lobulation tend to carry a great risk of misdiagnosis in morphologic assessments.

Keywords Three-dimensional time-of-flight magnetic resonance angiography · Unruptured intracranial aneurysms · Distal internal carotid artery · Morphologic assessment · Diagnostic accuracy

Abbreviations

3D-TOF-MRA	Three-dimensional time-of-flight magnetic resonance angiography
C5	Clinoid segment
C6	Ophthalmic segment
C7	Communicating segment
CI	Confidence interval
CVD	Cardiovascular disease
ICA	Internal carotid artery
MIP	Maximum intensity projection
OR	Odds ratio
UIAs	Unruptured intracranial aneurysms
VR	Volume-rendering

Key Points

1. Three-dimensional TOF-MRA provided high diagnostic confidence for detection of UIAs at the distal ICA.

✉ Yueqi Zhu
zhuyueqi@hotmail.com

[1] Department of Radiology, Shanghai Jiao Tong University Affiliated Sixth People's Hospital, No. 600, Yishan Road, 200233 Shanghai, China

2. Three-dimensional TOF-MRA could accurately display morphologic features.
3. Aneurysm size (tiny or giant) and sac shape (lobulation) were predictors of misdiagnosis in morphologic assessments.

Introduction

Unruptured intracranial aneurysms (UIAs) are relatively common in the general population (up to 5%) and are being increasingly diagnosed owing to the more frequent use of less invasive imaging techniques and higher image resolution [1]. Aneurysms arising from the segment of the internal carotid artery (ICA) between the proximal dural ring and bifurcation (C5–C7 segments of the ICA) constitute distal ICA aneurysms [2]. The distal portion of the ICA begins intracranially; hence, there is a risk of subarachnoid hemorrhage. Conventional catheter-based angiography with three-dimensional (3D) image reconstruction was considered the gold standard for detecting and evaluating intracranial aneurysms.; however, the invasive nature of this method, the use of radiation, the time required, and the risk of permanent neurological complications make it less than ideal as a screening tool and dynamic monitoring method for the long-term follow-up of patients with known aneurysms.

Noninvasive imaging tools, such as computed tomography angiography (CTA) or magnetic resonance angiography (MRA), are widely used for screening and triaging the management of UIAs [3, 4]. Distal ICA aneurysms are difficult to detect by CTA, as (a) there is a negative influence of bony structures that might fuse with aneurysms based on a defective segmentation threshold, (b) aneurysms in extremely twisted arteries are difficult to detect and (c) it is difficult to distinguish infundibular dilatation or the aneurysm-like basal portion of the branch [5, 6], especially for paraclinoid aneurysms, some of which at medial curves are highly vulnerable to a missed diagnosis due to the limitation of the partial volume effect [7]. In addition, an accurate morphologic assessment is based on detailed anatomical information regarding the configuration of the prominent lesion and location of the branch orifice, which are too delicate to be clearly determined by CTA [8]. Recent studies have indicated that magnetic resonance angiography (MRA) was a promising technique for aneurysm detection and growth follow-up. Meanwhile, MR scan with higher field intensity or gadolinium enhancement may increase the accuracy of aneurysm morphology display [9]. Three-dimensional time-of-flight MRA (3D-TOF-MRA) is a feasible technique for the detection of UIAs [10], eliminating the risks associated with contrast media and X-ray exposure. Although many reports have discussed the accuracy of TOF-MRA-based UIA diagnosis, few have addressed its diagnostic performance for UIAs at the ICA [4]. In the present study, we performed a comparative diagnostic accuracy analysis of 3D-TOF-MRA from three separate observers to assess UIAs at the distal ICA. Morphologic features were also collected for further analysis, and digital subtraction angiography (DSA) was used as the reference standard.

Material and Methods

Patients

This retrospective study was approved by the institutional review board. A total of 2947 patients who had known or were suspected of having cerebrovascular disease and underwent both MRA and DSA at our institution between January 2015 and May 2020 were included.

The main inclusion criteria were as follows: (a) patients who had known or were suspected of having cerebrovascular disease and underwent 3D-TOF-MRA and subsequent DSA and (b) those with aneurysms at segments C5–C7 of the ICA. The exclusion criteria consisted of the following: (a) patients who were proven to have subarachnoid hemorrhage (SAH) ($n=286$), (b) patients who underwent DSA prior to MRA ($n=68$), (c) DSA performed later than 3 months ($n=137$), (d) patients with incomplete clinical data or with poor image quality for diagnosis ($n=58$) and (e) patients with known or treated aneurysms (as per aneurysm exclusion) (Fig. 1).

Imaging Protocol of TOF-MRA

All MR angiographic examinations were performed with a 3.0-T system (Achieva X Series; Philips Medical Systems, Best, the Netherlands) with a Sense-Head-8 receiver head coil. The 3D TOF MR angiograms were obtained by using 3D T1-weighted fast field-echo sequences. The acquired image data sets were transferred to an extended workstation (EWS; Philips Medical Systems) and then processed to a volume-rendering (VR) image at 3D volume inspection (Philips Medical Systems). The maximum intensity projection (MIP) image was also reconstructed for the evaluation.

To reduce arterial overlay and for the efficient identification of aneurysms, we used the single artery highlighting method as described previously [11]. To locate the aneurysm accurately, we combined the source image to identify the structure adjacent to the distal ICA. We analyzed three vessels (the ICAs and the vertebrobasilar artery) in each patient from six basic views and from arbitrary angles to clearly depict the origins and morphologic features of the aneurysms.

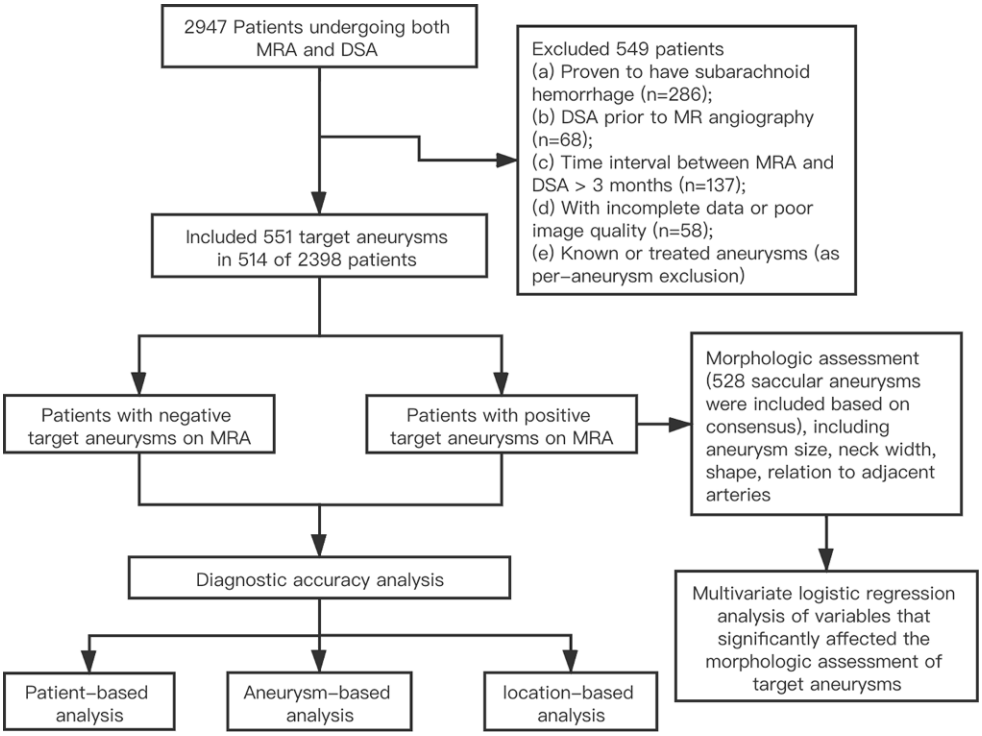

Fig. 1 Flowchart of this study. *MRA* magnetic resonance angiography, *DSA* digital subtraction angiography

Imaging Protocol of DSA

The DSA was performed within 3 months of MRA. Four vessels—the ICAs and the vertebral arteries on both sides—were catheterized for DSA. Posteroanterior and lateral projections were acquired with a biplanar unit (Artis zee; Siemens Healthcare, Forchheim, Germany) with a 1024 × 1024 matrix and a 17–20cm field of view in all patients. Rotational angiography was performed with an 8s 200° rotational run, acquiring 200 images; for affected arteries, further 3D images with VR reconstruction were produced on a workstation with a 128 × 128 × 128 to 512 × 512 × 512 matrix (Syngo XWP VA70B; Siemens Healthcare). Contrast medium (iodixanol; Henrui Medicine, Lianyungang, China) was injected for a total of 8 mL for the ICA (rate 4–5 mL/s), 6 mL for the vertebral artery (rate 2–3 mL/s), and 10–15 mL per artery for rotational angiography (rate 2–3 mL/s). Two experienced observers (B. Gu. and J. Zhao with 25 and 24 years of experience in interventional neuroradiology, respectively) evaluated the cerebral aneurysms together.

Image Review

Three board-certified observers (observers A, B, and C, Y. Zhu, H. Lu, and Y. Zhang, respectively, with 15, 20, and 7 years of experience in interventional neuroradiology, respectively) reviewed all MR images and were blinded to all clinical and DSA results. They analyzed all 3D-TOF-MRA with VR image data sets at an offline workstation from multiple on-screen viewing angles by using the single artery highlighting approach. The source images and maximum intensity projection images were presented on screen, allowing for adjustment of the appropriate threshold of the window width and window level to diagnose or differentiate aneurysms with infundibula. Cases of one or more aneurysms detected were considered positive; all others were considered negative (regardless of another cerebral vascular disease). For the morphologic assessment of 3D-TOF-MRA, the configuration of the aneurysm and its relationship to adjacent arteries were decided by a consensus among the three reviewers.

Definition

The classification of the ICA was based on 7-scale anatomically based nomenclature according to Bouthiller et al.'s classification [12]. Unruptured aneurysms on segments C5–C7 of the ICA were included in the present study. If a single aneurysm was located across more than one segment, the particular location of the main aneurysm body was recorded. The recorded morphologic features included aneurysm size, neck width, shape and relation to adjacent arteries. An aneurysm was considered giant if the greatest diameter was larger than 15 mm, large if it was 7–15 mm, small if it was between 3 and 7 mm, and tiny if it was less than 3.0 mm [13]. For assessment of aneurysm shape, three features were considered: the presence of a daughter

sac (an irregular protrusion from the wall of the aneurysm that was less than 25% of the total volume of the main sac), lobulation (a protuberance arising directly from the primary neck of the aneurysm or from the main body and representing 25% or more of the volume of the main sac), and margin (smooth or irregular). With respect to the relationship between the aneurysm and parent artery, there were two grades: (a) an aneurysm arising from the side wall of the artery and (b) an aneurysm arising from an arterial bifurcation. The latter could be of three types: (a) aneurysm neck arising from the angle of the bifurcation, (b) more than 75% of the aneurysm neck arising from one limb of the bifurcation, and (c) aneurysm involving the entire angle of the bifurcation. Precise morphologic display of the cerebral aneurysm on 3D-TOF-MRA was considered a failure if any of the morphologic parameters did not conform to the DSA findings. The detailed definition of the aforementioned parameters is specified in the online Supplement.

Table 1 Summary of patient characteristics with target aneurysms confirmed by DSA

Characteristic	Patients ($n = 514$)
Age (years), mean ± standard deviation	58.3 ± 11.8
Female sex, *n* (%)	320 (62.3)
Alcohol intake, *n* (%)	132 (25.7)
Current smoking, *n* (%)	125 (24.3)
Diabetes mellitus, *n* (%)	104 (20.2)
Hypertension, *n* (%)	258 (50.2)
Hypercholesterolemia, *n* (%)	67 (13.0)
History of cerebral infarction, *n* (%)	33 (6.4)
History of CVD, *n* (%)	45 (8.8)
Polycystic kidney, *n* (%)	3 (0.6)
Moyamoya, *n* (%)	5 (1.0)
Arteriovenous malformation, *n* (%)	3 (0.6)
Multiple intracranial aneurysms, *n* (%)	80 (15.6)

CVD cardiovascular disease, *DSA* digital subtraction angiography

Statistical Analysis

Categorical demographic and basic characteristic variables are expressed as numbers and percentages, while continuous variables are summarized as the means ± standard deviations. With DSA as the reference standard, the sensitivity, specificity, positive predictive value (PPV), negative predictive value (NPV) and accuracy of 3D-TOF-MRA for the evaluation of UIAs at the distal ICA were calculated on a patient-based, aneurysm-based and location-based basis with the 95% confidence interval by using the Wilson score method. Interobserver agreement is expressed as the Cohen κ value for categorical variables. For the patient-based evaluation, if a patient had multiple aneurysms and one of the target aneurysms was missed or overdiagnosed, this patient was considered to have false negative or false positive findings. Also, χ^2-tests were performed to compare the proportion of aneurysms detected by TOF-MRA and DSA for each aneurysm-specific variable, size, neck width (wide if >4 mm or fundus-to-neck ratio <2), shape (margin/daughter sac/lobulation) and relation to adjacent arteries. Multivariate logistic regression was used to identify the variables that significantly affected the morphologic assessment on 3D-TOF-MRA. Subgroup analysis was performed based on three specific locations. All analyses were performed by using statistical software (SPSS 22.0; IBM, Armonk, NY, USA), and $P < 0.05$ was considered to indicate a significant difference.

Results

Clinical Characteristics

According to the DSA results, of 2398 patients enrolled, 551 aneurysms in 514 patients (320 women, mean age 58.3 ± 11.8 years; range 27–85 years) were confirmed at the distal ICA. Patient characteristics are shown in Table 1. Of the 514 patients with target aneurysms, 481 had 1 aneurysm (47 had aneurysms at other locations), 29 had 2 target aneurysms (8 had aneurysms at other locations),

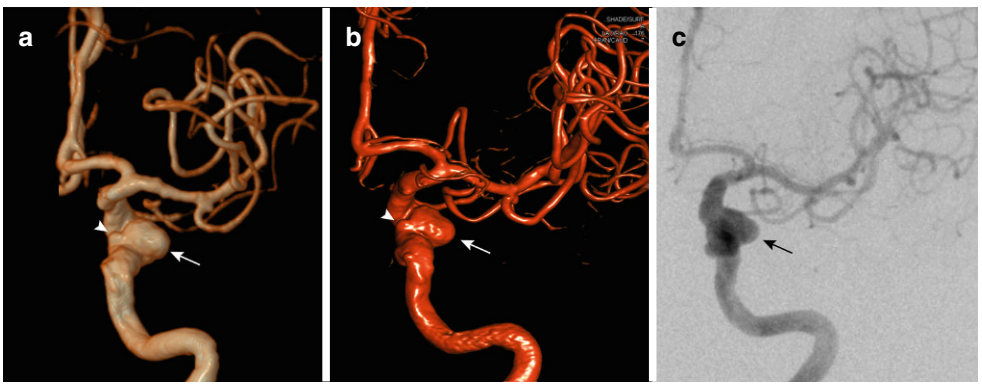

Fig. 2 Example of a patient with an aneurysm in the C6 segment of the left internal carotid artery (ICA). **a** Three-dimensional time-of-flight (TOF) MRA shows a 6×5×5 mm aneurysm (*arrow*) with a lobulated shape (*arrowhead*). DSA image with Volume-rendering (VR) reconstruction (**b**) and two-dimensional DSA image (**c**) show the aneurysm and its lobulated shape seen on 3DTOF-MRA with VR reconstruction

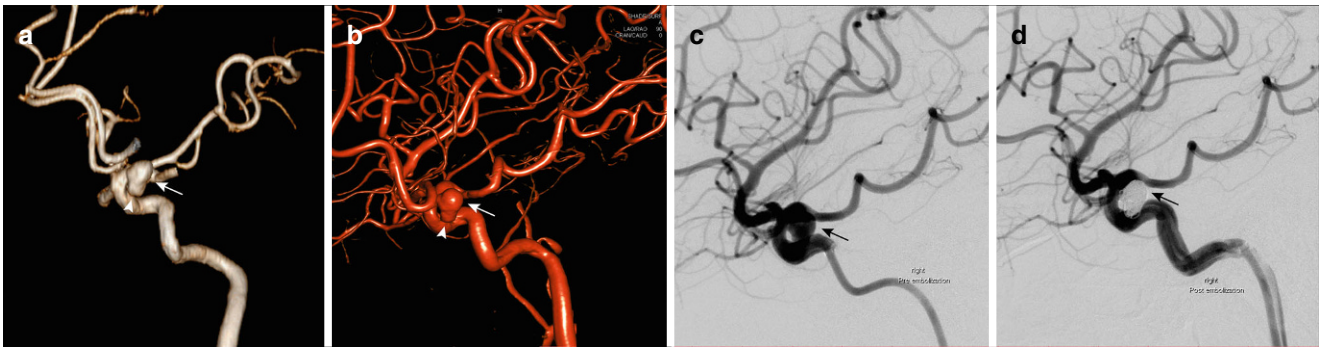

Fig. 3 Example of a patient with an aneurysm in the C7 segment of the right ICA. **a** Three-dimensional TOF-MRA shows a 4 × 6 × 4 mm aneurysm (*arrow*) with a lobulated shape (*arrowhead*). DSA image with VR reconstruction (**b**) and two-dimensional DSA image (**c**) show the aneurysm in the C7 segment of the right ICA. **d** DSA image shows total occlusion of the aneurysm after embolization with coils

and 4 had 3 target aneurysms. Of 551 target aneurysms, 52 (9.4%) were located at the C5 segment, 162 (29.4%) were located at C6 (Fig. 2), and 337 (61.2%) were located at C7 (Fig. 3). A total of 387 patients with 425 aneurysms identified on DSA at other sites and 1497 patients without aneurysms served as negative cases.

Diagnostic Performance of 3D-TOF-MRA

Three-dimensional TOF-MRA at 3.0-T revealed a high accuracy (98.4–98.9%), sensitivity (97.9–98.8%), and specificity (98.6–98.9%) for detection of distal ICA UIAs. Detailed evaluations are provided in Table 3 in Supplement. Excellent interobserver agreement was found on a per patient (mean κ = 0.959), per-aneurysm (mean κ = 0.942) and per location (mean κ = 0.966 for C5; mean κ = 0.958 for C6; and mean κ = 0.956 for C7) basis (Supplement).

Table 2 Aneurysm-specific characteristics on 3D-TOF-MRA and DSA

Morphologic characteristic	MRA ($n = 528$)	DSA ($n = 528$)	*P* Value
Aneurysm size	–	–	0.390
< 3 mm	63	46	–
3–6.99 mm	346	355	–
7–15 mm	96	103	–
> 15 mm	23	24	–
Neck	–	–	0.197
Thin neck	72	87	–
Wide neck	456	441	–
Aneurysm sac shape	–	–	0.306
Margin	427	407	–
Daughter sac	68	79	–
Lobulated	33	42	–
Aneurysm and side branches	–	–	0.875
Sidewall	275	271	–
Bifurcation tip	171	182	–
Involves one limb of the bifurcation	80	73	–
Involves the entire bifurcation	2	2	–

3D-TOF-MRA three-dimensional time-of-flight magnetic resonance angiography, *DSA* digital subtraction angiography

Morphologic Display of Aneurysms On 3D-TOF-MRA

A total of 537 target aneurysms were accurately diagnosed with both 3D-TOF-MRA and DSA: 528 saccular aneurysms, 3 dissection aneurysms, 4 pseudo or vesicular aneurysms and 2 fusiform aneurysms (Supplement). Then, 528 saccular aneurysms were included in the final morphologic assessment (Table 2 and Fig. 4). Three-dimensional TOF-MRA images were used to accurately characterize size in 94.9% (501 of 528) of aneurysms, neck width in 97.2% (513 of 528) of aneurysms, shape in 92.6% (489 of 528) of aneurysms and relation to adjacent vessels in 96.4% (509 of 528) of aneurysms. The χ^2-tests showed no significant difference between MRA and DSA in the proportion of aneurysms for each aneurysm-specific variable. Multivariate logistic regression analysis revealed that aneurysm size and sac shape significantly affected the morphologic assessment on 3D-TOF-MRA (Fig. 5). Binary logistic regression analysis showed that in the whole cohort, tiny (OR = 5.56; 95% CI = 2.32, 13.28; $P < 0.001$) or giant (OR = 3.52; 95% CI = 1.07, 11.64; $P = 0.039$) aneurysms and those with a lobulated sac shape (OR = 3.48; 95% CI = 1.43, 8.46; $P = 0.006$) had a significantly higher chance of having an inaccurate display of morphologic features on 3D-TOF-MRA than small-sized aneurysms or those with a margin. This is mainly due to blood flow signal lost in a tiny or giant aneurysm sac, and thus cause the sac display smaller in TOF-MRA than in DSA. In the subgroup analysis, tiny aneurysms (OR = 8.27; 95% CI = 2.65, 25.85; $P < 0.001$) and those with bifurcation involvement (OR = 3.86; 95% CI = 1.18, 12.63; $P = 0.026$) were associated with a significantly higher rate of misdiagnosis at C7, while aneurysms at C6 with a lobulated shape (OR = 4.42; 95% CI = 1.06, 18.52; $P = 0.04$) showed a negative correlation with an accurate morphologic assessment. These finding indicated

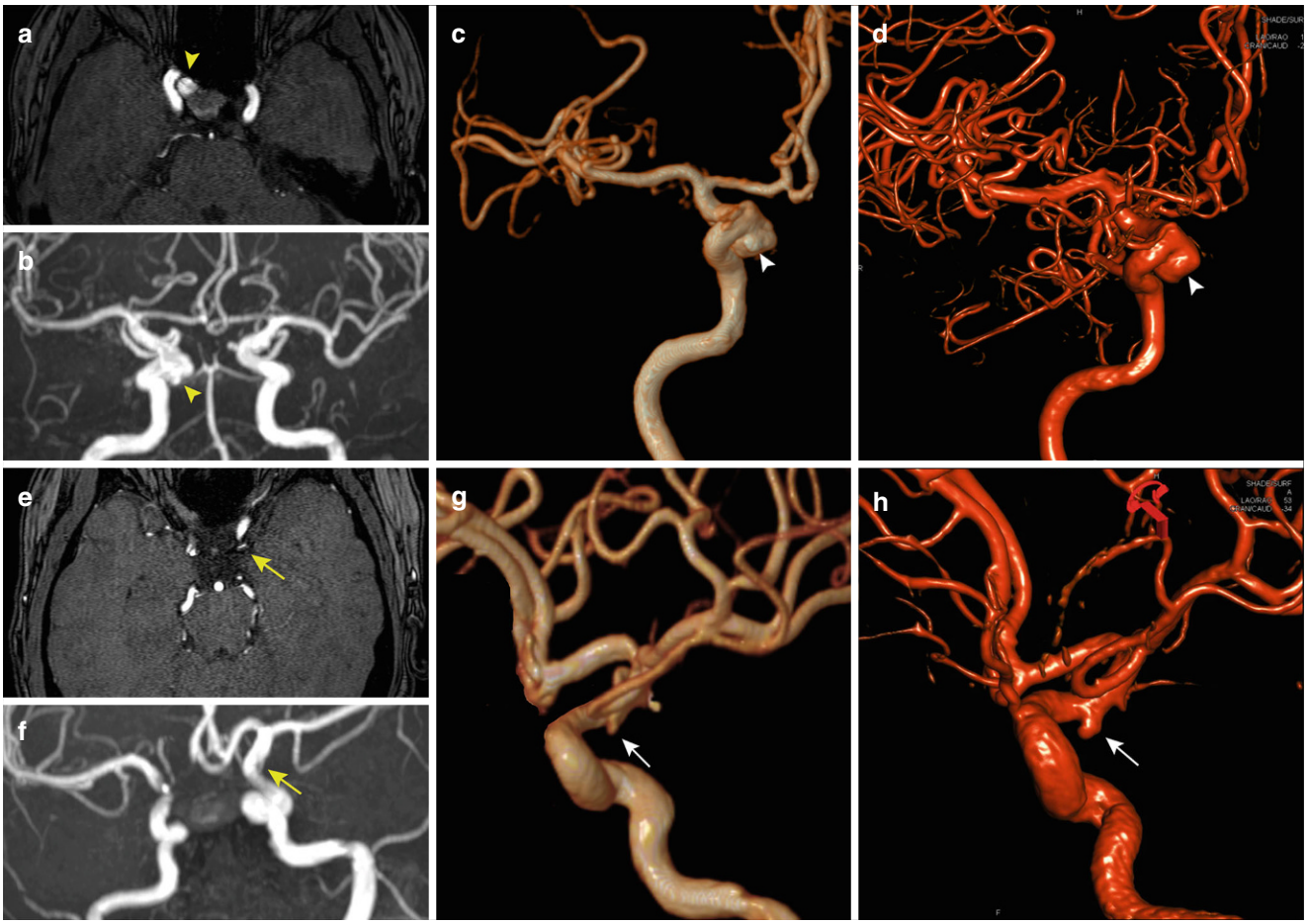

Fig. 4 Comparison between TOF-MRA and DSA image. An axial TOF-MRA source image (**a**), coronal MIP reconstruction (**b**) and VR reconstruction (**c**) show a small aneurysm with a daughter sac (*arrowhead*) while the sac cannot be appreciated by DSA image (**d**). An axial TOF MRA source image (**e**), coronal MIP reconstruction (**f**) and VR reconstruction (**g**) show an infundibular (*arrow*) while DSA image shows a tiny aneurysm (**h**)

that tiny aneurysms are often difficult to be distinguished from infundibula at C7 segmentation and aneurysm shape display may be greatly affected by the turbulent flow at C6 segmentation.

Discussion

Currently, there are a number of comparative diagnostic imaging investigations for UIAs. CTA is regarded as a convenient and reliable first-line modality to detect and triage the management of intracranial aneurysms, with reported overall sensitivities reaching up to 97% [3, 14]. Meanwhile, CTA is considered superior to determine sac patency of giant aneurysm than MRA or even DSA [15]; however, due to the complex bony structure of the skull base and distortion of the distal ICA, the diagnostic performance of CTA tended to be inferior to that on other locations [16, 17]. Yang et al. assessed the accuracy of CTA for the diagnosis of cerebral aneurysms 5 mm or smaller, showing sensitivities of 92.1% and 90.8% for aneurysms in the ICA and 95.6% and 95.8% for aneurysms in the anterior circulation, respectively. Diagnostic accuracy and sensitivity were even lower for aneurysms less than 3 mm in size or with an unruptured status (sensitivity 85.7% for < 3 mm vs. 95.1% for 3–5 mm and 90.3% for unruptured vs. 97.2% for ruptured) [18]. A previous study reported that a considerable portion of false positive lesions were more likely to found in the distal ICA region on TOF-MRA (77.8%, 14/18 on CTA vs. 93.3%, 14/15 on TOF-MRA) [19]. Concerning morphologic assessments, the aneurysm size measurement error on CTA seemed to be larger than that on TOF-MRA (3.8–4.0% vs. 0.8–3.0%) in an in vitro silicone model [20]. Until recently, little clinical information was available for the morphologic assessment of aneurysms on CTA. Hiratsuka et al. reported an evaluation of aneurysmal morphology between CTA and TOF-MRA and indicated that VR images showing TOF-MRA tended to have a slightly higher detection rate of aneurysms with an irregular shape (33/47 vs. 29/46 by CTA) and surface deformity

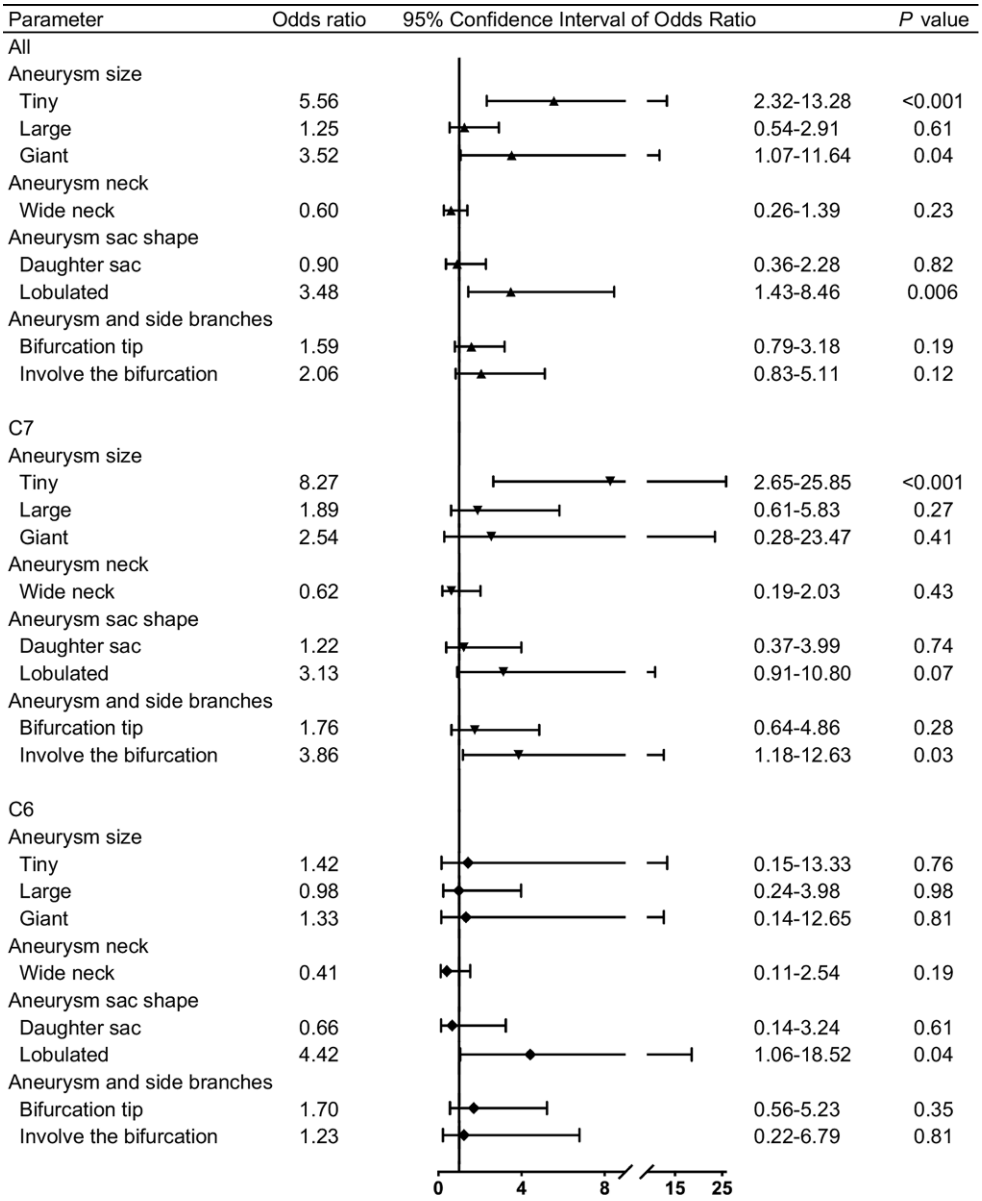

Fig. 5 Odds ratios for aneurysm-specific variables in the morphologic assessment and subgroup analysis of C7 and C6. Aneurysm size (tiny or giant) and relation to adjacent arteries (bifurcation tip) were the variables that significantly affected the morphologic assessment on 3D-TOF-MRA

were mainly caused by blood signal lost (39/47 vs. 31/46 by CTA) [19]. A misjudgment of aneurysm surface deformation could lead to an overdiagnosis of the rupture risk of UIAs [21]. In addition, inherent dual-phase imaging by CTA (possible disparity between scan time and contrast enhancement in aneurysm), along with bone removal applications, would inevitably result in information reduction or a prolonged scan time and increased radiation dose (range from 20–25% above the level of the standard dose) [6].

In our retrospective study, we demonstrated that 3D-TOF-MRA could accurately depict and display UIAs at the distal ICA. We believed that 3D-TOF-MRA had remarkable superiority in imaging quality at the distal ICA by avoiding artifacts of the skull base and eliminating the risks posed by contrast media and X-ray exposure. On morphologic assessments, over 90% of aneurysm-specific variables (94.9% size, 97.2% neck width, 92.6% shape and 96.4% relation to adjacent vessels) were accurately characterized, and no significant difference between MRA and DSA was revealed. We systematically evaluated each parameter in the logistic equation and defined small size, the presence of a margin, sac shape and sidewall relation to adjacent arteries as dummy variables for analysis. Indicator comparisons in the whole cohort showed that tiny or giant aneurysms and those with a lobulated sac shape had a significantly higher chance of having an inaccurate display of morphologic features than small aneurysms or those with a margin. These findings were consistent with the previously reported higher diagnostic reliability of 3D-TOF-MRA for medium-sized aneurysms [2, 22]. For aneurysms less than 3 mm in size, it

may be difficult to eliminate the error of size measurement, while for large or giant aneurysms, intravoxel spin-phase dispersion and saturation associated with slow and turbulent flow with signal loss may prevent adequate demonstration of the entire aneurysm [23]. This could result in potential errors in image interpretation for TOF-MRA. In the subgroup analysis of C7, we found that tiny size ($P<0.001$) or bifurcation involvement ($P=0.03$) also significantly affected the morphological assessment. These results could be explained by the high proportion of infundibular dilatation or complex vascular anatomy, which increased the difficulty in describing a specific aneurysm shape rather than just judging whether an aneurysm existed [24]. We demonstrated that a lobulated sac shape was another parameter that was associated with a significantly high rate of morphologic misdiagnosis in both the whole distal ICA aneurysm ($P=0.006$) and those in segment C6 ($P=0.04$). A previous study of paraclinoid aneurysms revealed that type II aneurysms (based on Barami's classification) arising from the ventral ophthalmic segment of the ICA were vulnerable to turbulent flow and signal loss in the assessment of the aneurysm sac [25]. The lobulated sac shape of distal ICA aneurysms on 3D-TOF-MRA may reflect either focal weakening with subsequent extreme distention of the aneurysm wall or could be explained by partial thrombosis in the sac because TOF-MRA is simply a cast of the aneurysm lumen rather than an image of the actual aneurysm wall [26]. Both focal wall degeneration and luminal thrombosis of the sac shape are relatively difficult to display on 3D-TOF-MRA. In addition, because of the extremely limited number of incorrectly diagnosed cases (only 5), the subgroup of aneurysms located in segment C5 was not subjected to regression analysis. Therefore, when we clarified risk factors that were associated with an inaccurate display of the morphologic features of aneurysms, 3D-TOF-MRA tended to be less reliable than DSA.

We acknowledge that the limitations of our study include its retrospective design, which may be characterized by limited availability of data and susceptibility to information biases. It is inevitable that some patients with negative findings on TOF-MRA did not undergo DSA, which may have affected the sensitivity and negative predictive value of MRA relative to DSA. Additionally, aneurysms in our imaging data were not measured quantitatively, which may account for the low diagnostic performance of the morphologic features size and neck width. Lastly, TOF-MRA often requires more examination time, which is much longer than CTA scan and the image quality of TOF-MRA is more likely to be affected by blood flow at curved vessel, thus displaying the shape or diameter of an aneurysm is often inferior to CE-MRA or CTA [15].

In conclusion, this large cohort study showed that 3D-TOF-MRA at 3.0-T had a relatively high diagnostic accuracy for the detection and display of morphologic features of UIAs at the distal ICA. We believe that 3D-TOF-MRA is a safe replacement for invasive DSA and superior to CTA in the diagnostic work-up of patients with distal ICA aneurysms.

Supplementary Information The online version of this article (https://doi.org/10.1007/s00062-021-01076-4) contains supplementary material, which is available to authorized users.

Funding This study received funding by 1) National Key Research and Development Program (No. 2017YFC0109204); 2) Shanghai Municipal Education Commission-Gaofeng Clinical Medicine Grant Support (No.20152528); 3) Shanghai Jiao Tong University "Medical and Research" Program (ZH2018ZDA19).

Declarations

Conflict of interest G. He, J. Wang, Y. Zhang, M. Li, H. Lu, Y. Cheng and Y. Zhu declare that they have no competing interests.

Ethical standards For this article no studies with human participants or animals were performed by any of the authors. All studies performed were in accordance with the ethical standards indicated in each case. Institutional Review Board approval was obtained. Informed consent: written informed consent was waived.

References

1. Etminan N, Rinkel GJ. Unruptured intracranial aneurysms: development, rupture and preventive management. Nat Rev Neurol. 2016;12:699–713.
2. Imaizumi Y, Mizutani T, Shimizu K, Sato Y, Taguchi J. Detection rates and sites of unruptured intracranial aneurysms according to sex and age: an analysis of MR angiography-based brain examinations of 4070 healthy Japanese adults. J Neurosurg. 2018;130:573–8.
3. Menke J, Larsen J, Kallenberg K. Diagnosing cerebral aneurysms by computed tomographic angiography: meta-analysis. Ann Neurol. 2011;69:646–54.
4. Sailer AM, Wagemans BA, Nelemans PJ, de Graaf R, van Zwam WH. Diagnosing intracranial aneurysms with MR angiography: systematic review and meta-analysis. Stroke. 2014;45:119–26.
5. Chen W, Xing W, He Z, Peng Y, Wang C, Wang Q. Accuracy of 320-detector row nonsubtracted and subtracted volume CT angiography in evaluating small cerebral aneurysms. J Neurosurg. 2017;127:725–31.
6. Romijn M, Gratama van Andel HA, van Walderveen MA, Sprengers ME, van Rijn JC, van Rooij WJ, Venema HW, Grimbergen CA, den Heeten GJ, Majoie CB. Diagnostic accuracy of CT angiography with matched mask bone elimination for detection of intracranial aneurysms: comparison with digital subtraction angiography and 3D rotational angiography. AJNR Am J Neuroradiol. 2008;29:134–9.
7. Liao CH, Lin CJ, Lin CF, Huang HY, Chen MH, Hsu SP, Shih YH. Comparison of the effectiveness of using the optic strut and tuberculum sellae as radiological landmarks in diagnosing paraclinoid aneurysms with CT angiography. J Neurosurg. 2016;125:275–82.
8. Lindgren AE, Koivisto T, Björkman J, von Und Zu Fraunberg M, Helin K, Jääskeläinen JE, Frösen J. Irregular Shape of Intracranial

Aneurysm Indicates Rupture Risk Irrespective of Size in a Population-Based Cohort. Stroke. 2016;47:1219–26.
9. Nakagawa D, Nagahama Y, Policeni BA, Raghavan ML, Dillard SI, Schumacher AL, Sarathy S, Dlouhy BJ, Wilson S, Allan L, Woo HH, Huston J, Cloft HJ, Wintermark M, Torner JC, Brown RD, Hasan DM. Accuracy of detecting enlargement of aneurysms using different MRI modalities and measurement protocols. J Neurosurg. 2018;130:559–65.
10. Malhotra A, Wu X, Forman HP, Matouk CC, Gandhi D, Sanelli P. Management of tiny unruptured intracranial aneurysms: a comparative effectiveness analysis. JAMA Neurol. 2018;75:27–34.
11. Li M, Zhu Y, Song H, Gu B, Lu H, Li Y, Tan H, Cheng Y. Subarachnoid Hemorrhage in Patients with Good Clinical Grade: Accuracy of 3.0-T MR Angiography for Detection and Characterization. Radiology. 2017;284:191–9.
12. Bouthillier A, van Loveren HR, Keller JT. Segments of the internal carotid artery: a new classification. Neurosurgery. 1996;38:425–32. discussion 432–423.
13. van Rooij WJ, Sluzewski M. Endovascular treatment of large and giant aneurysms. AJNR Am J Neuroradiol. 2009;30:12–8.
14. Chappell ET, Moure FC, Good MC. Comparison of computed tomographic angiography with digital subtraction angiography in the diagnosis of cerebral aneurysms: a meta-analysis. Neurosurgery. 2003;52:624–31. discussion 630–621.
15. Wang X, Benson J, Jagadeesan B, McKinney A. Giant cerebral aneurysms: comparing CTA, MRA, and digital subtraction angiography assessments. J Neuroimaging. 2020;30:335–41.
16. Philipp LR, McCracken DJ, McCracken CE, Halani SH, Lovasik BP, Salehani AA, Boulter JH, Cawley CM, Grossberg JA, Barrow DL, Pradilla G. Comparison Between CTA and Digital Subtraction Angiography in the Diagnosis of Ruptured Aneurysms. Neurosurgery. 2017;80:769–77.
17. van Asch CJ, Velthuis BK, Rinkel GJ, Algra A, de Kort GA, Witkamp TD, de Ridder JC, van Nieuwenhuizen KM, de Leeuw FE, Schonewille WJ, de Kort PL, Dippel DW, Raaymakers TW, Hofmeijer J, Wermer MJ, Kerkhoff H, Jellema K, Bronner IM, Remmers MJ, Bienfait HP, Witjes RJ, Greving JP, Klijn CJ; DIAGRAM Investigators. Diagnostic yield and accuracy of CT angiography, MR angiography, and digital subtraction angiography for detection of macrovascular causes of intracerebral haemorrhage: prospective, multicentre cohort study. BMJ. 2015;351:h5762.
18. Yang ZL, Ni QQ, Schoepf UJ, De Cecco CN, Lin H, Duguay TM, Zhou CS, Zhao YE, Lu GM, Zhang LJ. Small Intracranial Aneurysms: Diagnostic Accuracy of CT Angiography. Radiology. 2017;285:941–52.
19. Hiratsuka Y, Miki H, Kiriyama I, Kikuchi K, Takahashi S, Matsubara I, Sadamoto K, Mochizuki T. Diagnosis of unruptured intracranial aneurysms: 3T MR angiography versus 64-channel multi-detector row CT angiography. Magn Reson Med Sci. 2008;7:169–78.
20. Ramachandran M, Retarekar R, Harbaugh RE, Hasan D, Policeni B, Rosenwasser R, Ogilvy C, Raghavan ML. Sensitivity of Quantified Intracranial Aneurysm Geometry to Imaging Modality. Cardiovasc Eng Technol. 2013;4:75–86.
21. Mocco J, Brown RD Jr, Torner JC, Capuano AW, Fargen KM, Raghavan ML, Piepgras DG, Meissner I, Huston J III; International Study of Unruptured Intracranial Aneurysms Investigators. Aneurysm Morphology and Prediction of Rupture: An International Study of Unruptured Intracranial Aneurysms Analysis. Neurosurgery. 2018;82:491–6.
22. Li MH, Cheng YS, Li YD, Fang C, Chen SW, Wang W, Hu DJ, Xu HW. Large-cohort comparison between three-dimensional time-of-flight magnetic resonance and rotational digital subtraction angiographies in intracranial aneurysm detection. Stroke. 2009;40:3127–9.
23. Zhu C, Wang X, Eisenmenger L, Tian B, Liu Q, Degnan AJ, Hess C, Saloner D, Lu J. Surveillance of Unruptured Intracranial Saccular Aneurysms Using Noncontrast 3D-Black-Blood MRI: Comparison of 3D-TOF and Contrast-Enhanced MRA with 3D-DSA. AJNR Am J Neuroradiol. 2019;40:960–6.
24. Chen CJ, Moosa S, Ding D, Raper DM, Burke RM, Lee CC, Chivukula S, Wang TR, Starke RM, Crowley RW, Liu KC. Infundibular dilations of the posterior communicating arteries: pathogenesis, anatomical variants, aneurysm formation, and subarachnoid hemorrhage. J Neurointerv Surg. 2016;8:791–5.
25. Kinouchi H, Mizoi K, Nagamine Y, Yanagida N, Mikawa S, Suzuki A, Sasajima T, Yoshimoto T. Anterior paraclinoid aneurysms. J Neurosurg. 2002;96:1000—5.
26. Björkman J, Frösen J, Tähtinen O, Backes D, Huttunen T, Harju J, Huttunen J, Kurki MI, von Und Zu Fraunberg M, Koivisto T, Manninen H, Jääskeläinen JE, Lindgren AE. Irregular Shape Identifies Ruptured Intracranial Aneurysm in Subarachnoid Hemorrhage Patients With Multiple Aneurysms. Stroke. 2017;48:1986–9.